Electronic Supplementary Material (ESI) for Nanoscale.

Electronic Supplementary Information: A Classical Picture of Subnanometer Junctions: an Atomistic Drude Approach to Nanoplasmonics

Tommaso Giovannini,[†] Marta Rosa,[‡] Stefano Corni,[*,‡,¶] and Chiara Cappelli[*,†]

†*Scuola Normale Superiore, Piazza dei Cavalieri 7, 56126 Pisa, Italy.*

‡*Department of Chemical Sciences, University of Padova, via Marzolo 1, Padova, Italy*

¶*CNR Institute of Nanoscience, via Campi 213/A, Modena, Italy*

E-mail: stefano.corni@unipd.it; chiara.cappelli@sns.it

S1 Fluctuating Charges Force Field

The goal of the Fluctuating Charge (FQ) Force Field (FF) [1–3] is to provide a way to accurately describe electrostatic interactions between atoms. To this end, each atom is endowed with a charge (q) which is not fixed, but can vary according to the Electronegativity Equalization Principle (EEP), which states that at the equilibrium all atoms have the same electronegativity, i.e. differences in electronegativity drive the flux of charge and thus polarization between atoms.

For a given set of N atoms, the FQ energy functional can be defined in terms of electronegativities and chemical hardnesses. In particular, the FQ energy functional is obtained by defining the energy in terms of a Taylor expansion with respect to charges:

$$E = \sum_i \frac{\partial E}{\partial q_i} q_i + \sum_i \frac{\partial^2 E}{\partial {q_i}^2} q_i^2 + \sum_{i \neq j} J_{ij} q_i q_j \tag{S1}$$

where energy first and second derivatives with respect to charges define the electronegativity χ and chemical hardness η, respectively. The last term of the equation takes into account charge interactions. By imposing the diagonal terms of the interaction matrix J to be atomic chemical harnesses, the above equation can be rewritten in the following form:

$$\begin{aligned} F(\mathbf{q}, \lambda) =& \sum_i^N q_i \chi_i + \frac{1}{2} \sum_i^N \sum_j^N q_i J_{ij} q_j + \lambda (\sum_i^N q_i - Q_{tot}) \\ =& \mathbf{q}^\dagger \boldsymbol{\chi} + \frac{1}{2} \mathbf{q}^\dagger \mathbf{J} \mathbf{q} + \boldsymbol{\lambda}^\dagger \mathbf{q} \end{aligned} \tag{S2}$$

where the Latin index i runs over the atoms. $\boldsymbol{\lambda}$ is a set of Lagrangian multipliers used to impose the total charge conservation. $\mathbf{J}$ is the charge interaction kernel as defined above.

Several ways have been proposed in the literature to define $\mathbf{J}$ in order to avoid the so called "polarization catastrophe".[4] Remarkably, in this paper, the charges q are not simply defined as point-like FQ charges,[5] but a charge distribution function (an s-type Gaussian function)

is instead assigned to each atom. Such a choice permits easy and efficient computation of the interaction kernel J, by exploiting the machinery developed in common quantum chemistry codes. In fact, the integrals that need to be calculated read:

$$J_{ij}(r_{ij}) = \int_{\mathbb{R}^3} d\mathbf{r} \int_{\mathbb{R}^3} d\mathbf{r}' \frac{|\varphi_i(\mathbf{r}-\mathbf{r}_i)|^2 |\varphi_j(\mathbf{r}'-\mathbf{r}_j)|^2}{|\mathbf{r}-\mathbf{r}'|} = \frac{1}{r_{ij}} \mathrm{erf}\left(\frac{r_{ij}}{\sqrt{R_i^2+R_j^2}}\right) \tag{S3}$$

where

$$\varphi(\mathbf{r}-\mathbf{r}_i) = \frac{1}{(R_i^2\pi)^{3/2}} e^{-\frac{|\mathbf{r}-\mathbf{r}_i|^2}{R_i^2}}$$

$r_{ij} = |\mathbf{r}_i - \mathbf{r}_j|$ is the distance between a pair of FQs and R_i is the width of the Gaussian distribution, which can be obtained by imposing the diagonal term of the matrix to correspond to the atomic chemical hardness:

$$\lim_{r_j \to r_i} \frac{1}{r_{ij}} \mathrm{erf}\left(\frac{r_{ij}}{\sqrt{R_i^2+R_j^2}}\right) = \eta_i \Longrightarrow R_i = \sqrt{\frac{2}{\pi}} \frac{1}{\eta}$$

The stationarity conditions of the functional in Eq. S2 are defined by the following equations:

$$\begin{cases} \sum_j J_{i,j} q_j + \lambda = -\chi_i \\ \\ \sum_i q_i = Q_{tot} \end{cases} \tag{S4}$$

The previous system of equations can be recast in a more compact formalism by introducing the extended $\mathbf{D}$ matrix:

$$\mathbf{D} = \left(\begin{array}{c|c} \mathbf{J} & \mathbf{1_\lambda} \\ \hline \mathbf{1_\lambda^\dagger} & \mathbf{0} \end{array}\right)$$

where $\mathbf{1}_\lambda$ is a rectangular matrix containing the Lagrangian multipliers. The linear system of equation then reads:

$$\mathbf{D q_\lambda} = -\mathbf{C}_Q \tag{S5}$$

where $\mathbf{C}_Q$ collects atomic electronegativities and total charge constraints, whereas charges and Lagrange multipliers are collected in $\mathbf{q}_{\boldsymbol{\lambda}}$. $\mathbf{D}$ includes the $\mathbf{J}$ matrix and the Lagrangian blocks.

S2 Linear Response Equations

S2.1 Static Response

In order to calculate static response properties (such as the system polarizability), Eq.S5 has to be modified. In particular, in the case of one-metal nanoparticles, all the atoms are of the same type, and thus no polarization occurs due to differences in atomic electronegativies, which in the pristine FQ model define the polarization "source" in the Maxwell's meaning of the term. However, the system polarizes under the effect of a static external electric field. Static response equations are derived by simply adding to the whole energy a term accounting for the interaction with the external electric field. It is worth noticing that this can be in principle achieved either by defining the external perturbation in terms of an electric field, or an associated electric potential. Since FQ is defined in terms of charges, the use of the potential V^{ext} is more convenient.

Thus, Eq. S2 becomes:

$$F(\mathbf{q},\lambda) = \mathbf{q}^\dagger\boldsymbol{\chi} + \frac{1}{2}\mathbf{q}^\dagger\mathbf{J}\mathbf{q} + \boldsymbol{\lambda}^\dagger\mathbf{q} + \mathbf{q}^\dagger\mathbf{V}^{ext} \tag{S6}$$

By minimizing $F(\mathbf{q},\lambda)$, the static response equations are obtained:

$$\mathbf{D}\mathbf{q}_{\boldsymbol{\lambda}} = -\mathbf{C}_Q - \mathbf{V}^{ext} \tag{S7}$$

Once FQ charges are calculated by solving Eq. S7, the static polarizability can be calculated by evaluating the induced dipole moment.

Notice also that standard FQ equations can be reformulated by introducing the electrochem-

ical potential μ_i^{el}:

$$F = \sum_i (q_i\chi_i + \frac{1}{2}q_i\eta_i q_i + V_i q_i) \tag{S8}$$

$$V_i = V_i^{ext} + \sum_{k\neq i} J_{ik}q_k \tag{S9}$$

$$\mu_i^{el} = \frac{\partial F}{\partial q_i} = \chi_i + q_i\eta_i + V_i \tag{S10}$$

where J_{ik} is the proper electrostatic non-diagonal matrix element (i.e., the Gaussian kernel defined in Eq. S3).

S2.2 Frequency dependent Response

When nanoparticles of finite dimension are irradiated by an external oscillating electric field, local plasmons arise.

Because in the FQ approach a charge is placed on each atom, the frequency-dependent response of the system is defined once the variation of the charges in time is obtained. In our newly developed ωFQ model, we assume electron transfer to occur under two alternative regimes:

- Conductive regime: the exchange of electrons between contiguous atoms is governed by the dynamics of the delocalized conduction electrons, giving rise to a damping.
- Tunneling regime: the conductive exchange of electrons between the atoms is mediated by a quantum tunneling mechanism.

These two different regimes were considered in order to obtain the final equation of ωFQ approach as exposed in the main text (see Eqs. 5,6,7). Starting from Eq. 6, the complex linear equation that is needed to be solved in order to obtain the complex electric charges is:

$$\sum_j \left(-\sum_k K_{ik}^{\text{tot}} D_{ij} + \sum_k K_{ik}^{\text{tot}} D_{kj} + i\omega\delta_{ij} \right) q_j = \sum_j (V_i^{ext} - V_j^{ext}) K_{ij}^{\text{tot}} \tag{S11}$$

Once ωFQ frequency-dependent charges are obtained by solving Eq. S11, the complex polarizability $\overline{\alpha}$ is easily calculated. In particular, starting from the charges, the complex electric dipole $\overline{\boldsymbol{\mu}}$ is calculated:

$$\overline{\boldsymbol{\mu}} = \sum_i q_i \cdot \mathbf{r}_i \tag{S12}$$

where $\mathbf{r}_i$ is the distance between the atom i-th and the origin. From the complex dipole moment, the complex polarizability $\overline{\alpha}$ is calculated by solving:

$$\overline{\alpha}_{kl} = \frac{\partial \overline{\boldsymbol{\mu}}_k}{\partial \mathbf{E}_l} = \sum_i q_i \cdot \frac{\mathbf{k}_i}{E_l} \tag{S13}$$

where k and l are x,y,z directions. From such a quantity, the absorption cross section is recovered:

$$\sigma_{\text{abs}} = \frac{4\pi}{3c} \omega \ \text{tr}\big(\text{Im}\overline{\alpha}\big) \tag{S14}$$

where c is the speed of light, ω is the external frequency and $\text{Im}\overline{\alpha}$ is the imaginary part of the complex polarizability $\overline{\alpha}$.

S2.3 Calculation of the electric current

To calculate the electric current that flows across the studied systems, we have reformulated for the atomistic case what already reported by Marchesin *et al.*[6] in case of *ab-initio* calculations. Since we are dealing with a finite object we can use the continuity equation to define the current that flows across a plane perpendicular to the dimer axis and passing through the center of the junction (see Fig.S1). ωFQ calculations yield complex response charges to an external monochromatic field in the frequency domain. The continuity equation gives a

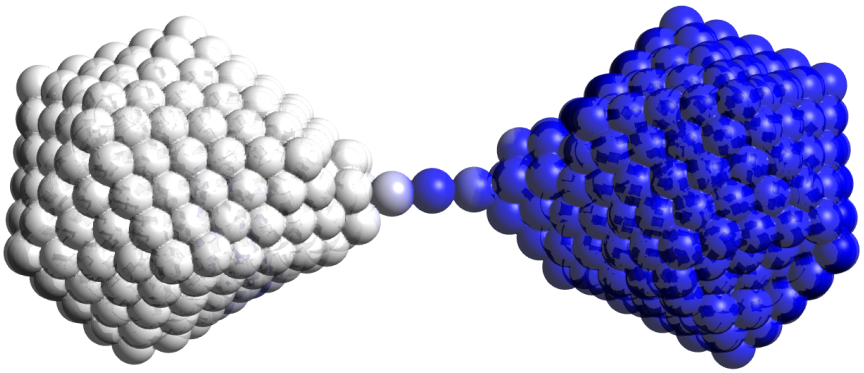

Figure S1: Pictorial view of a dimer junction. Charges on the blue atoms are those considered in the definition of the electric current (Eq.S15).

relation between the total induced charge and the current flowing across the junction $I(t)$ at time t. By referring for instance to the dimer junction in Fig.S1, the most intuitive way of calculating the current is to only consider charges belonging to one of the two regions of the dimer, for instance those assigned to the blue atoms. In the frequency domain, the current can be obtained as:

$$I(\omega) = -i\omega \sum_i q_i(\omega) \tag{S15}$$

Therefore, the modulus of the current (maximum current) flowing across the junction in response to a given external electric field $\mathbf{E} = \mathbf{E_0}\cos(\omega t)$ reads:

$$|I_{max}(\omega)| = \omega \sqrt{\sum_i \Big(Re(q_i^2(\omega)) + Im(q_i^2(\omega)) \Big)} \tag{S16}$$

In this paper, the current is calculated for any of the plasmon resonances for each geometry of the two systems under investigation.

S3 Computational Details

ωFQ has been implemented in a stand-alone program, named nanoFQ written in Fortran77. The final equation S11 is directly solved by an LU decomposition (by exploiting ZSYSV

Lapack subroutine),[7] however the computational time can be further reduced by iterative methods for solving complex linear equations involving a sparse matrix.[8] This will be considered in future works.

S4 Model Parametrization

ωFQ was tested against sodium nanoparticles (see below), which have been chosen because of their simple electronic structure (only one valence electron is present on each atom). Eq. 4 depends on several parameters, which were recovered from the literature whenever possible or were fitted to reproduce reference *ab-initio* plasmonic energy of selected spherical sodium nanoparticles (vide infra). Such parameters are summarized in Table S1.

Table S1: ωFQ parameters for sodium nanoparticles used in this paper. t.w.: this work. All data are given in atomic units.

Parameter	Eq.	Value (a.u.)	Ref
η	S7	0.292	t.w.
τ	5	1323	[9]
σ_0	5	5.21	[10]
A_{ij}	5	12.08	t.w.
d	7	12.0	t.w.
s	7	1.1	t.w.
l^0_{ij}	7	6.92	[10]

S4.1 Single Sodium Nanoparticles

ωFQ was first tested against selected sodium clusters (see Table S2) in order to assign the parameters entering ωFQ equations. Such parameters were defined as the best set to reproduce reference *ab-initio* plasmon resonances (ω_{ref}). The differences between ωFQ (ω) and reference values (ω_{ref}) can be inferred by data reported in table S2 and also depicted in Figure S2.

As it comes out evident, our choice of the model parameters makes ωFQ able to reproduce the plasmon resonance almost perfectly for most of the selected nanoparticles. Almost perfect

Table S2: Calculated ωFQ (ω) and reference values (ω_{ref}) plasmonic resonances for selected sodium clusters. The method used in case of reference values is also reported.
[a] plan-wave DFT calculations performed with Quantum Espresso, LDA xc functional, ultrasoft pseudopotential, plane wave cut-off of 35 Ry (140 Ry on the density), TDDFT calculations with the Lanczos Liouville approach TurboTDDFT[15,16]
[b] Sodium spherical nanoparticle of 10 nm diameter.

Na_N	Method	ω_{ref} (eV)	ω (eV)
15	TDLDA[11]	2.75	2.80
59	TDDFT[a]	2.20	2.28
169	TDLDA[11]	3.01	3.09
331	TDLDA[12]	2.98	3.06
331	TDLDA[11]	3.06	3.06
331	jellium[12]	3.17	3.06
832	jellium[13]	3.25	3.21
1000	jellium[14]	3.30	3.21
13803	Mie[b]	3.30	3.30

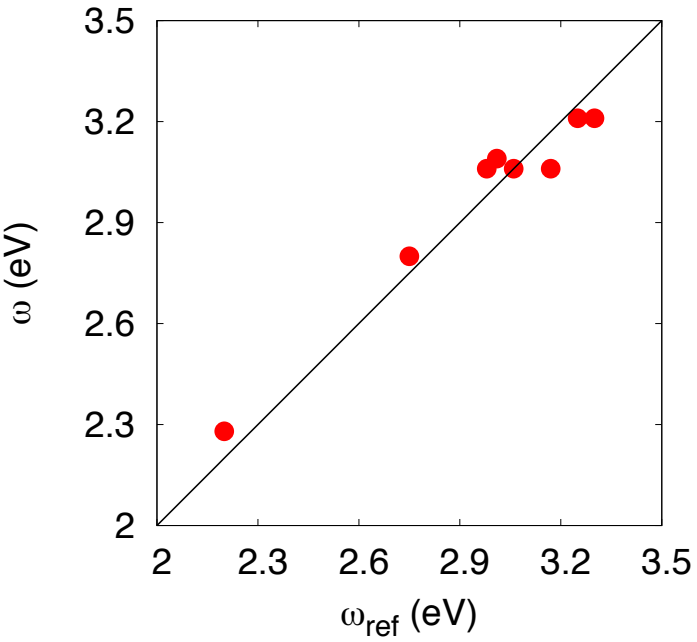

Figure S2: Graphical depiction of ωFQ (ω) and reference values (ω_{ref}) for the sodium clusters reported in Table S2. The slope of the dotted line is 0.99

linearity with respect to the reference *ab-initio* data is also reported (the slope of the dotted line is 0.99). It is also worth stressing that such results show that the free parameters of ωFQ, i.e. those which cannot be recovered from the literature, can easily be determined once the optical properties of small nanoparticles are known. This means that the extension of the model to nanomaterials based on other kind of metal atoms would simply require the knowledge of the associated plasmon resonances. However, as stated in the main text ωFQ needs to be properly extended to account for the atomic core polarizability that characterizes d-metals.

To show the computational advantages of using a classical approach such as ωFQ with respect to *ab-initio* approaches, we report in Table S3 computational time together with the memory used in case of Na_59 cluster. Notice that, as stated in section S3, nanoFQ solves Eq. S11 for each frequency given as input. In this case, we have calculated the plasmonic response of Na_{59} by considering 300 frequencies in input, from 0.0 to 3.0 eV with a step of 0.01 eV. The results reported in Table S3 refer to the total computational time.

Table S3: [a] MacBook Pro 2011, 2,3 GHz Intel Core i5, 4GB RAM. 4 cores used for OpenMP parallelization. [b] Intel Xeon X5650 2.6 GHz, 12 cores, 48 GB RAM

	RAM	computational time
ωFQ[a]	1.3 MB	0.534 s
TDDFT[b]	900 MB	2 h

In addition, to demonstrate the applicability of the code to large nanoparticles we have performed a calculation on a 10 nm diameter sodium nanoparticle (13803 atoms, see Table S2 and Figure S3), by putting 200 frequencies as input (from 2.0 to 4.0 eV, 0.01 eV steps). We have exploited an Intel(R) Xeon(R) CPU E5-2667 v2 @ 3.30GHz, 16 cores, 128 GB RAM machine, by requiring 8 cores for OpenMP parallelization. The computational time was 191h and the memory (RAM) used was 60.72 GB. We want to remark here that the computational cost of our approach scales as O(N3) due to the fact that the equation S11 is solved by an LU decomposition. We are working on the implementation of an iterative scheme to solve Eq. S11, which will reduce the computational cost to O(N2).

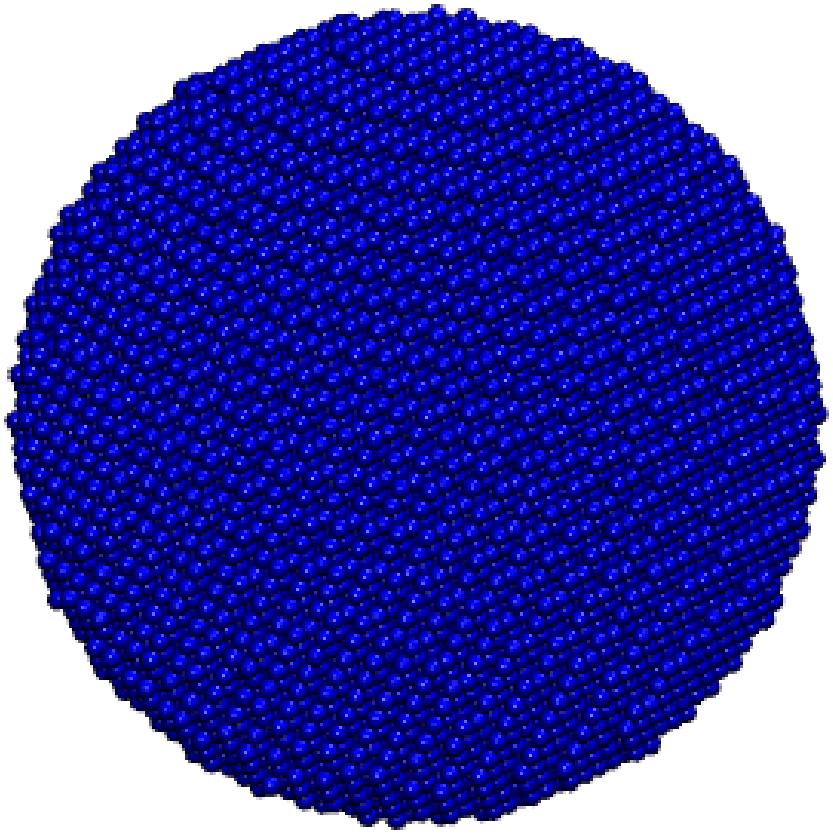

Figure S3: Graphical depiction of a 10 nm diameter spherical sodium nanoparticle (13803 atoms)

S4.2 Test on Single Silver Nanorods

In order to show the applicability of ωFQ to the case of *d*-metals nanoparticles, Silver nanorods of different size were selected because the absorption maxima are far from interband transitions.[17] Nanorod structures have been constructed by using OpenMD[18] nanorod_pentBuilder functionality, by imposing the lattice constant to be equal 4.08 Å. ωFQ parameters are reported in Table S4.

Table S4: ωFQ parameters for silver nanoparticles used in this paper. t.w.: this work. All data are given in atomic units.

Parameter	Eq.	Value (a.u.)	Ref
η	S7	0.379	t.w.
τ	5	1200	[9]
σ_0	5	13.7	[10]
A_{ij}	5	15.46	t.w.
d	7	12.0	t.w.
s	7	0.92	t.w.
l^0_{ij}	7	5.45	[17]

ωFQ results are reported in Figure S4 (panel a), together with *ab-initio* data reproduced from Ref.[17] (panel b, red curve).

As it is evident, ωFQ spectra are in excellent agreement with *ab-initio* reference data.

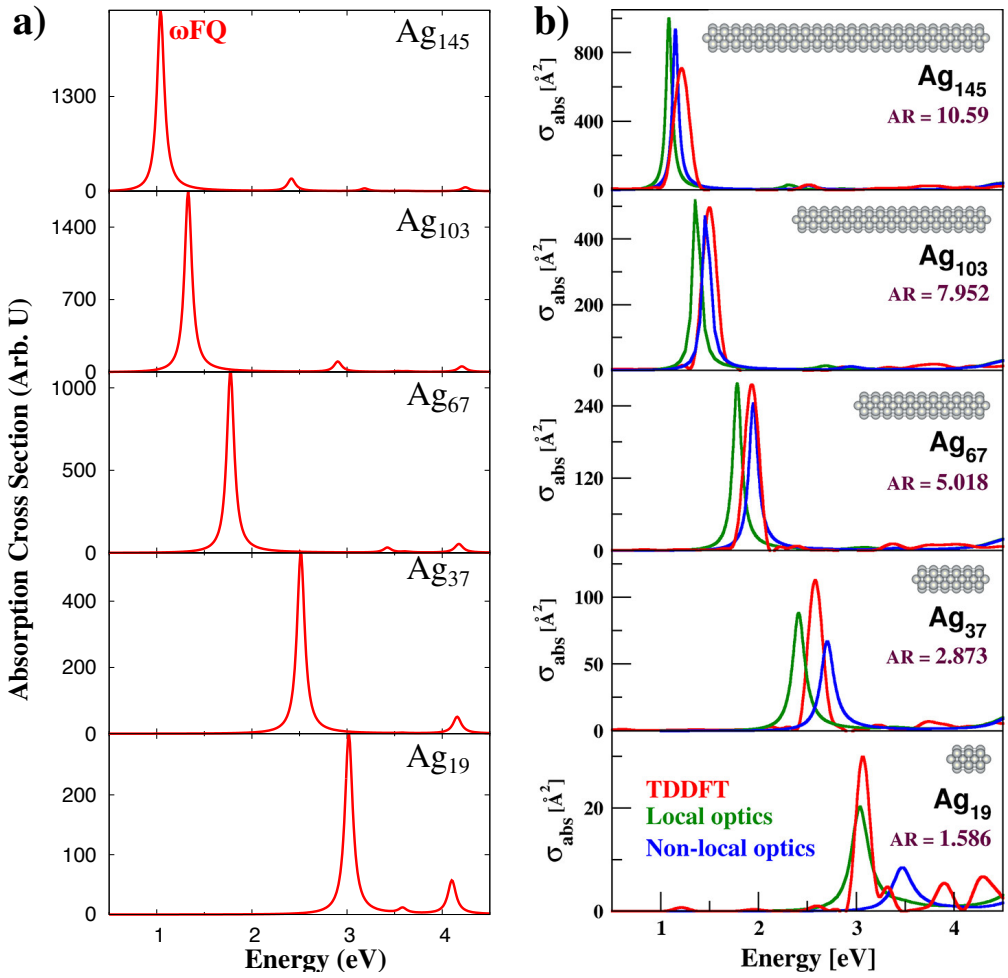

Figure S4: ωFQ (panel a) and reference (panel b) absorption cross sections for silver nanorods with different size. Reference *ab-initio* data (panel b, red curve) taken from Ref.[17]

S4.3 Dependence of ωFQ absorption cross sections on the choice of the model parameters

Among the several parameters defining our ωFQ model, n_0 is the one determining the absorption resonance (see Eq. 5). Thus, because n_0 is defined as the ratio between the static conductance σ_0 and the damping τ, such a ratio needs to remain constant in order to guarantee the plasmon resonance to stay the same. The results obtained by varying both σ_0 and τ, but keeping their ratio fixed are shown in the left panel of Figure S5. The different curves were obtained by multiplying σ_0 and τ by the factor shown in the key. As expected, the curves become thinner and the limit of the stick spectrum is recovered as the ratio doubles or triplicates. On the other hand, if the values of σ_0 and τ decrease by a factor 3 or 10, the curve broadens, thus recovering the artificial broadening usually employed to plot *ab-initio* calculations.

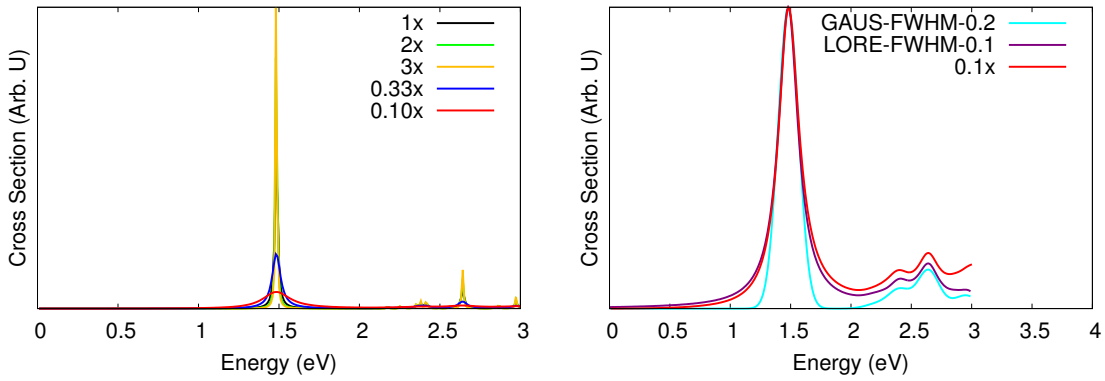

Figure S5: (left): calculated ωFQ absorption cross sections as a function of the multiplicative factor of σ_0 and τ; (right): Gaussian or Lorentzian convolution of ωFQ stick compared with ωFQ spectrum obtained with factor=0.1

To further investigate the behavior of our model, ωFQ stick values were convoluted with a Lorentzian or a Gaussian-type function, with Full Width at Half Maximum (FWHM) of 0.1 and 0.2 eV, respectively. It is evident from the inspection of the right panel of Fig.S5 that the Lorentzian function best fits ωFQ values obtained with a factor of 0.1. This is not surprising, if Eq. 5 is inspected. On the basis of the data shown above, all the spectra

reported in the paper were obtained by keeping σ_0 and τ to the literature values and to convolute each stick spectrum with a Lorentzian function. In this way, ωFQ spectra are coherent with the corresponding *ab-initio* values.

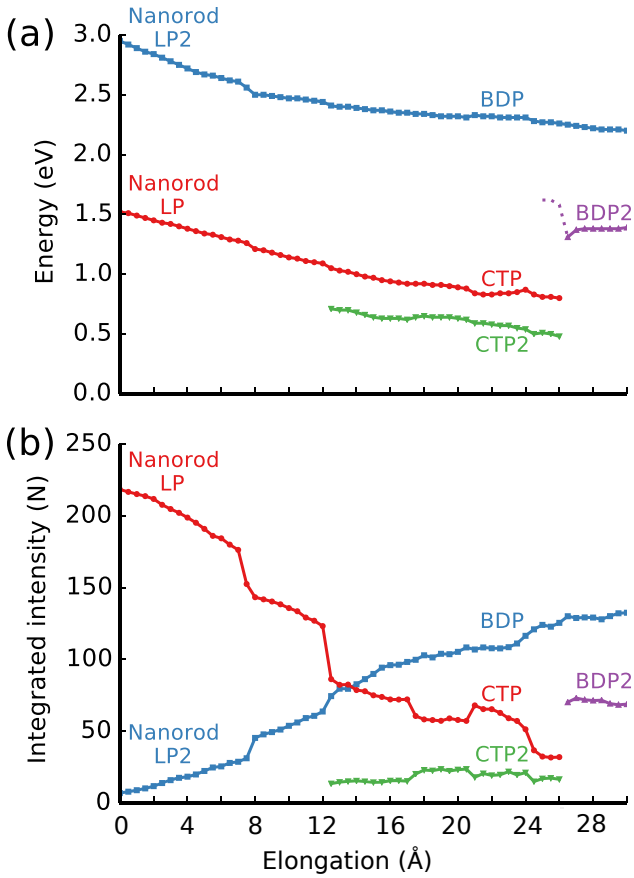

Figure S6: Analysis of the plasmon resonances during the nanorod elongation. (a) Energy maxima and (b) integrated intensity (i.e., the area underlying the curve) of the plasmon modes as a function of d. The intensities are normalized so that the full spectrum integrates to the number of valence electrons (261). The line labels correspond to the labeling used in Fig. 1(b) and labels A–H to the geometries shown in Fig. 1 (main text).
Figure reproduced from Ref.[19]

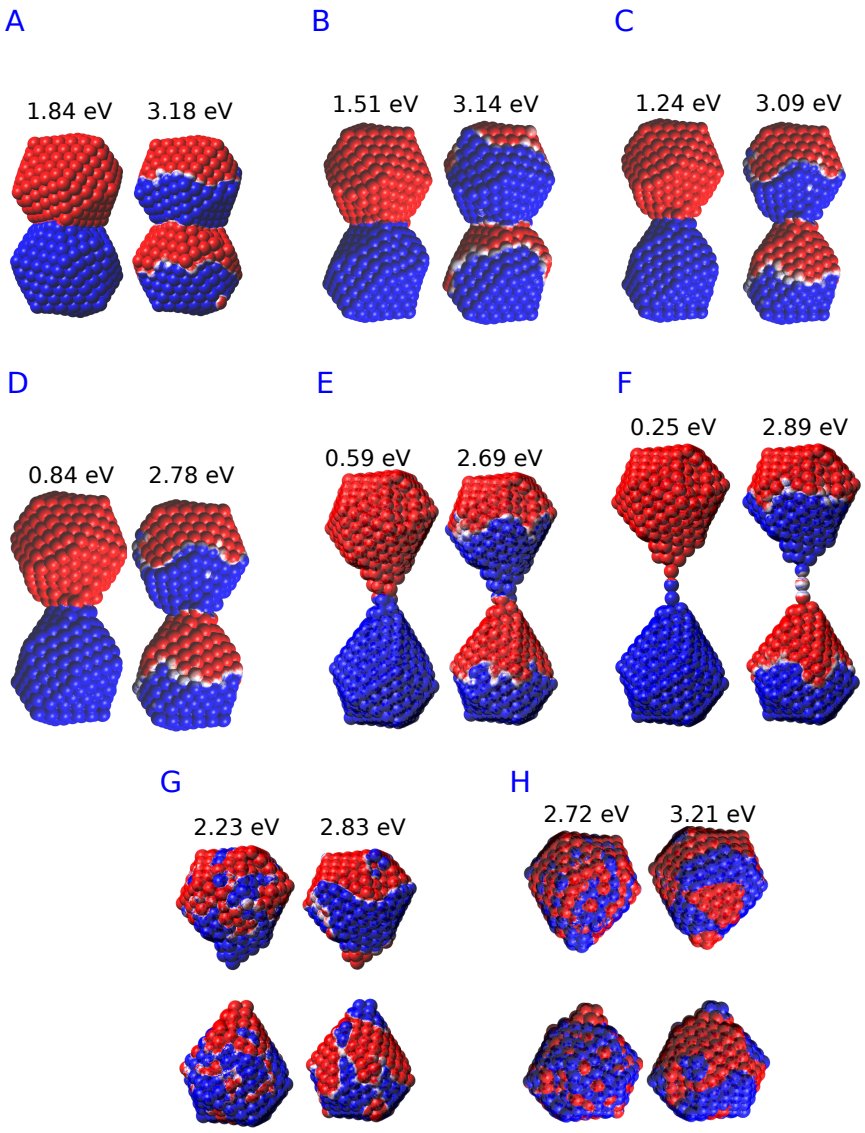

Figure S7: ωFQ MEP maps for plasmon excitations (eV) of selected structures A-H. The nominal gap distances d are (from A to H): 3.7, 9.7, 14.7, 22.7, 25.9, 32.1, 32.3, 34.1 Å. Blue color indicates a negative charge, whereas red color indicates a positive charge.

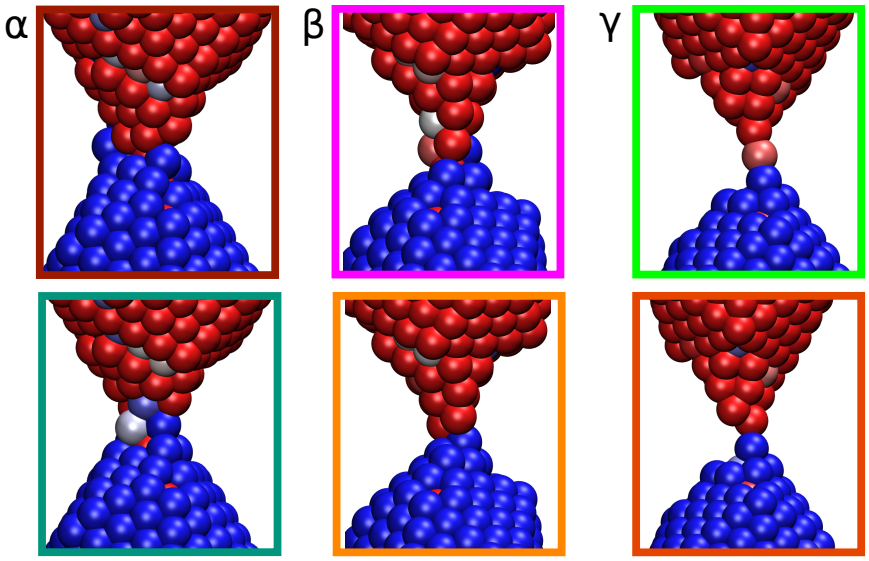

Figure S8: ωFQ imaginary charges on the junction atoms before (top) and after (bottom) the α, β and γ spectral jumps. Blue color indicates a negative charge, whereas red color indicates a positive charge.

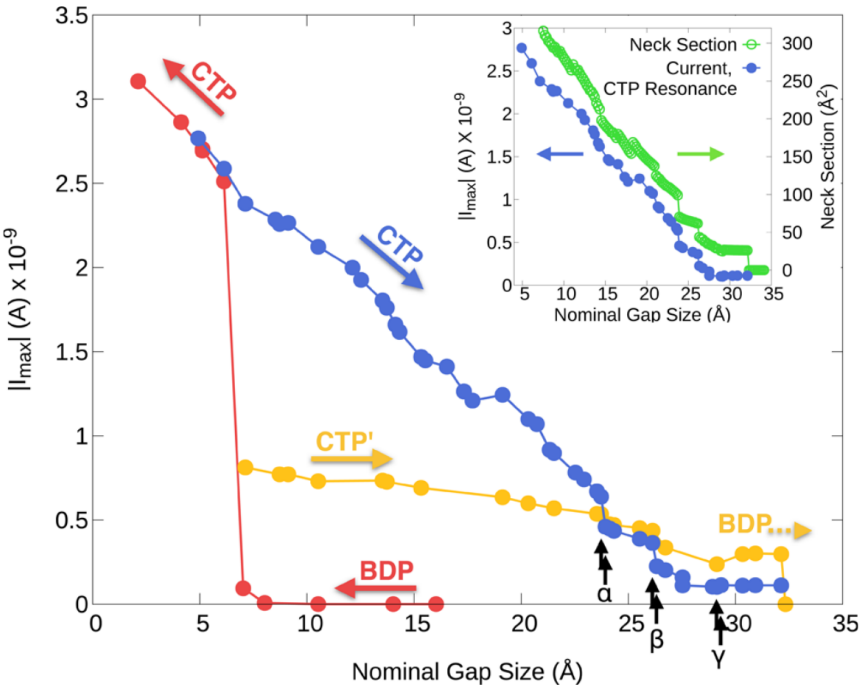

Figure S9: DFT absolute value of the electric current through the plasmonic nanojunction as a function of the elongation distance. Colored arrows indicate the direction of the process (approaching, in red, and retracting, in blue and orange). Black arrows indicate the position of the α β and γ spectral jumps. Data reproduced from Ref.[6]

References

(1) Rick, S. W.; Stuart, S. J.; Berne, B. J. *J. Chem. Phys.* **1994**, *101*, 6141–6156.

(2) Rick, S. W.; Stuart, S. J.; Bader, J. S.; Berne, B. J. *J. Mol. Liq.* **1995**, *65-66*, 31–40.

(3) Rick, S. W.; Berne, B. J. *J. Am. Chem. Soc.* **1996**, *118*, 672–679.

(4) Jensen, L. L.; Jensen, L. *J. Phys. Chem. C* **2008**, *112*, 15697–15703.

(5) Cappelli, C. *Int. J. Quantum Chem.* **2016**, *116*, 1532–1542.

(6) Marchesin, F.; Koval, P.; Barbry, M.; Aizpurua, J.; Sánchez-Portal, D. *ACS Photonics* **2016**, *3*, 269–277.

(7) Bartels, R. H.; Golub, G. H. *Communications of the ACM* **1969**, *12*, 266–268.

(8) Saad, Y. *Iterative methods for sparse linear systems*; siam, 2003; Vol. 82.

(9) Palik, E. D. *Handbook of optical constants of solids*; Elsevier, 1997.

(10) Haynes, W. *CRC Handbook of Chemistry and Physics*; CRC Press: Boca Raton, 2014.

(11) Li, J.-H.; Hayashi, M.; Guo, G.-Y. *Phys. Rev. B* **2013**, *88*, 155437.

(12) Zhang, P.; Feist, J.; Rubio, A.; García-González, P.; García-Vidal, F. *Phys. Rev. B* **2014**, *90*, 161407.

(13) Weick, G.; Ingold, G.-L.; Jalabert, R. A.; Weinmann, D. *Phys. Rev. B* **2006**, *74*, 165421.

(14) Varas, A.; García-González, P.; Feist, J.; García-Vidal, F.; Rubio, A. *Nanophotonics* **2016**, *5*, 409–426.

(15) Rocca, D.; Gebauer, R.; Saad, Y.; Baroni, S. *J. Chem. Phys.* **2008**, *128*, 154105.

(16) Malcıoğlu, O. B.; Gebauer, R.; Rocca, D.; Baroni, S. *Comput. Phys. Commun.* **2011**, *182*, 1744–1754.

(17) Sinha-Roy, R.; Garcia-Gonzalez, P.; Weissker, H.-C.; Rabilloud, F.; Fernandez-Dominguez, A. I. *ACS Photonics* **2017**, *4*, 1484–1493.

(18) Gezelter, J.; Kuang, S.; Marr, J.; Stocker, K.; Li, C.; Vardeman, C.; Lin, T.; Fennell, C.; Sun, X.; Daily, K.; Zheng, Y.; Meineke, M. OpenMD, an open source engine for molecular dynamics. 2010.

(19) Rossi, T. P.; Zugarramurdi, A.; Puska, M. J.; Nieminen, R. M. *Phys. Rev. Lett.* **2015**, *115*, 236804.